Mechanical Systems and Signal Processing 120 (2019) 341–355

Contents lists available at ScienceDirect

Mechanical Systems and Signal Processing

journal homepage: www.elsevier.com/locate/ymssp

An approach based on expectation-maximization algorithm for parameter estimation of Lamb wave signals

Hongbo Jia [a], Zhichun Zhang [a], Hongwei Liu [a], Fuhong Dai [a], Yanju Liu [b], Jinsong Leng [a,*]

[a] Center for Composite Materials and Structures, Harbin Institute of Technology, Harbin 150080, PR China
[b] Department of Astronautical Science and Mechanics, Harbin Institute of Technology, Harbin 150080, PR China

ARTICLE INFO

Article history:
Received 13 April 2018
Received in revised form 29 September 2018
Accepted 19 October 2018

Keywords:
Lamb wave
Gabor pulse
EM algorithm
Dispersion effect
Multi-mode characteristic
Parameter estimation

ABSTRACT

In the structural health monitoring or nondestructive examination system based on the Lamb wave technology, the accurate and valid characteristics of wave packet extracted from the signal are critical factors to evaluate damage. However, the dispersion effect and the multi-mode characteristic in the elastic wave make the data extraction difficult and degrade the resolution, and therefore further prevent the effectiveness of Lamb wave for damage detection. In this study, we proposed a model-based approach for extracting effective characteristics from the noisy signals. By taking the narrow band Gabor pulse as the incident pulse and considering the general non-linear frequency dispersion (*quadratic dispersion*), we developed a model with five parameters to model the dispersive wave packet and obtained the parameter vector of each wave packet by the expectation-maximization (EM) algorithm. The parameters in the model present the characteristics of signals, which can be further applied to locate and evaluate the structure's damage. To study the convergence property, synthetic signals with different sampling rates and noise intensities were considered. Furthermore the developed approach is also verified by the experimental data from an isotropic aluminum plate.

1. Introduction

Lamb waves are guided waves propagating in plate-like structures, also known as plate waves [1]. For damage diagnosis of large plate-like structures, with the merits of long propagation distance without much energy loss and sensitivity to both internal and surface defects, the structural health monitoring (SHM) or nondestructive examination (NDE) based on Lamb wave is widely considered to be promising [2–4]. For active Lamb wave technology, the initial ultrasonic elastic wave is usually generated by the actuator mounted on or embedded in the monitored structure. Reflection/scattering occurs when the elastic wave encounters the damage or boundaries, which can be revealed by signal analysis. The extracted arrival time of wave packet can be used to locate the damage by classical methods such as ellipse method and triangulation method [5,6], and the mode information can be used for damage identification based on the scattering analysis [7,8]. For damage diagnosis in large structures, guided waves can be generated by the actuator on the surface of (or inside) the testing structure, instead of scanning the whole surface by the conventional ultrasonic test. Since the propagation medium of Lamb waves is the plate-like structure with the free upper and lower boundaries, the effect of the defects in/on the structure can be located and analyzed by analyzing the signals. By the Lamb wave technique, the rapid inspection of the monitored structure can be realized.

* Corresponding author.
E-mail address: lengjs@hit.edu.cn (J. Leng).

https://doi.org/10.1016/j.ymssp.2018.10.020
0888-3270/

However, in the Lamb wave testing, the nature of dispersion increases the signal duration and decreases the amplitude. Due to the interaction between the damage and the structure, the reflected wave packets may overlap seriously in the obtained signal. In practice, the background noise leads to the weak signal-to-noise ratio (SNR) and makes the problem more challenging. Thus, all these factors make the signal less straightforward and difficult to read. As another major problem, multi-mode characteristic has yet to be addressed through the application. Even at low frequency-thickness product, A0 and S0 modes can propagate in the structure, and with the increase of frequency-thickness product, more modes may complicate the signal. For these reasons, it is generally to excite a single mode with frequencies restricted in a relatively non-dispersive region in the tests. Even so, modal conversion will induce other modes that differ from the excitation, so the problem of the multi-mode characteristic is unavoidable. Indeed, the identification of modes different from the excitation can be used to recognize the damage type and help to understand the interaction between incident wave and damage.

Various techniques of signal processing have been proposed for the dispersive guided wave signals. One is time–frequency analysis, which employed short-time Fourier transform (STFT), Wigner-Ville distribution (WVD), Wavelet transform (WT) and Hilbert-Huang transform (HHT) [9–13]. Although the time–frequency analysis can provide an intuitive interpretation for the dispersive signals, the results may not be satisfactory since the time–frequency resolutions are very sensitive to the noise. The compressing techniques to increase the time resolution and SNR, with a known/measured dispersion relation to compensate the spread wave packets to the original shape, have been proven as effective methods [14–18]. Generally speaking, these techniques only compress the wave packets with the same mode as excitation, and the compensation results of other wave packets (*e.g.*, induced by the modal conversion phenomenon) are usually undesirable. To search better resolutions, matching pursuit (MP) and warped basis pursuit (W-BP) as a kind of sparse approximation or representation method has been employed in the guided wave signal processing [8,19–23]. In these techniques, dictionaries need to be carefully customized for decomposing the wave packet with several specific modes from the signal, *i.e.*, the time resolution strongly depends on the dictionary. Therefore, there is a critical need to develop a signal processing technique to obtain the accurate wave packet characteristics from the measured signal.

The model-based method that has to synthesize the physical characteristics of the system can be used for accurately extracting the wave packets characteristics and effectively applied in the processing non-dispersive signals [24–26]. Compared to the non-dispersive elastic wave, the guided wave should consider the dispersion effect. That is, besides the parameters of amplitude, time of arrive (ToA), center frequency, bandwidth and the phase, the dispersive characteristic must be considered. These features can be characterized by many methods, *e.g.*, the ToA can be carried out by the envelope or time–frequency analysis result (*i.e.* the time point responding to the energy peak); the frequency component distribution can be observed in the STFT or WVD results, etc. However, these methods have limitations in accuracy. In Lamb-wave-based defect inspection, the model-based compressive sensing (TS) technique adopting the warped frequency transform (WFT) technique were developed, and high solution were performed [27]. To achieve the application of the model-based method for time-domain signal analyzing, an effective and valid model is needed. In this paper, we take the narrowband Gabor pulse as the incident pulse and consider the general non-linear frequency dispersion to derive the model function strictly. With this model and parameter estimation method, the parameters in the measured signals can be calculated, and the estimation can be realized by the expectation-maximization (EM) algorithm.

This paper is organized as follows. In the Section 2, we developed the model function and showed how to identify the packet mode by determining the parameters and the implementation steps. In Section 3, synthetic signals with different SRs and noise intensities were used to study the convergence property; two groups of experimental data were measured from two isotropic aluminum plates: the first group was used to study the relationship between the result accuracy and the bandwidth of excitation pulse; the second group was used to verify the ability of mode identification and time locating.

2. Approach of dispersive signal processing based on the EM algorithm

In this section, we solved the problems in the Lamb wave signal from the model-based estimation perspective which can offer a more specific and a higher-resolution result. Actually, a parametric form of the dispersive wave packets can simplify the problems, and evaluate the structural damage based on signal characteristics conveniently.

2.1. Dispersive wave packets model

Since the time and frequency localization of the incident pulse are very important when using Lamb wave technology for efficient damage inspection, to select an optimal pulse as the excitation signal is a matter of cardinal significance [20]. To achieve the targets, the Gabor pulse (modulated Gaussian pulse) centered at a center frequency $2\pi f_c$ was employed here

$$f(t) = A\exp(-t^2/2\sigma^2)\cos(2\pi f_c t + \phi) \tag{1}$$

where the A is the amplitude, σ is a bandwidth factor that denotes the duration of the pulse waveform, ϕ is the phase, and t is the time.

With the assumption in the close region of high wave energy intensity, the dispersion relation characteristic can be adequately approximated by a finite polynomial. So the waveform of general non-linear frequency dispersion (the case of *quadratic dispersion*) can be given in [16], expressed as

$$f(x,t) = [m(t-k_1x) \otimes q(t)]\exp[i(2\pi f_c t - k_0 x)], \tag{2}$$

where $\otimes$ denotes convolution, $m(t)$ is a modulation envelope function related to the excitation signal, and $q(t)$ is a Gaussian function, expressed as,

$$q(t) = \sqrt{\alpha/\pi}\exp(-\alpha t^2), \tag{3}$$

where $\alpha = (4ik_2x)^{-1}$, $k_i (i = 0,1,2)$ are the Taylor series coefficients of the wave number that expanded by a Taylor series in the neighborhood of the center frequency $2\pi f_c$.$\tau = k_1 x$, where τ is defined as the ToA of wave packet. So the Eq. (2) can be rewritten as

$$f(\tau,t) = [m(t-\tau) \otimes q(t)]\exp[i2\pi f_c \cdot (t-\tau) + i\phi'], \tag{4}$$

where $\phi' = (2\pi f_c - k_0/k_1)\tau$. By using the Gabor pulse in Eq. (1) with initial phase $\phi = 0$ as the excitation signal, the waveform expression in Eq. (4) is,

$$f(\tau,t) = \sqrt{(g_1(\tau) - ig_2(\tau))}\exp\left[-(t-\tau)^2\beta g_1(\tau)\right]\exp\left\{i\left[2\pi f_c \cdot (t-\tau) + g_2(\tau)\cdot(t-\tau)^2 + \phi'\right]\right\}, \tag{5}$$

where $\beta = 1/2\sigma^2$, $g_j(\tau)$ $(j = 1,2)$ are the functions of ToA τ, which contain unknown Taylor coefficients $k_i (i = 1,2)$, given by

$$g_1(\tau) = \frac{k_1^2}{k_1^2 + (4\beta\tau k_2)^2}; \quad g_2(\tau) = \frac{4\beta^2\tau k_2 k_1}{k_1^2 + (4\beta\tau k_2)^2}, \tag{6}$$

Eqs. (5) and (6) indicate the duration of the wave packet increases with time, while the amplitude decreases. The description is consistent with the dispersive effect, and the real-valued waveform in the Eq. (5) of wave packet can be further simplified as

$$f(\tau,t) = f_A(\tau)\exp\left[-(t-\tau)^2\beta g_1(\tau)\right]\cos\left[g_2(\tau)\cdot(t-\tau)^2 + 2\pi f_c \cdot (t-\tau) + \varphi(\tau)\right], \tag{7}$$

where the $f_A(\tau)$ is the amplitude of wave packet and $\varphi(\tau)$ is the phase, both of which are the function of ToA. However, in the engineering application, the characteristics of flaw will affect the amplitude and may cause a phase variation. For simplification, we consider these functions irrelevant to the ToA. Therefore, the parametric model of general non-linear frequency dispersion wave packets can be expressed as

$$v(\Theta;t) = \xi\exp\left[-\beta\delta\cdot(t-\tau)^2\right]\cos\left[2\pi f_c \cdot \left(c\cdot(t-\tau)^2 + (t-\tau)\right) + \varphi\right], \tag{8}$$

where $\Theta = [\xi\ \delta\ \tau\ c\ \varphi]$ is the parameter vector, which contains all the parameters to describe the dispersive wave packets, the amplitude ξ, the bandwidth impact factor δ, the τ, the phase φ and the *mode characteristic constant* c. In addition, theoretically, the δ equals to $g_1(\tau)$, and $c = g_2(\tau)/2\pi f_c$. For simplifying the problem we consider the δ and c as parameters irrelevant to the τ.

For describing the multiple packets in the signal, the Eq. (8) can be generalized as

$$y(t) = \sum_{m=1}^{M} v(\Theta_m;t), \tag{9}$$

where $\Theta_m = [\xi_m\ \delta_m\ \tau_m\ c_m\ \varphi_m]$, and the M denotes the wave packet number in the noiseless signal.

2.2. Mode identification

In a given frequency region, since the dispersion relation characteristic of each mode is different, the unique mode's feature can be treated as the mode identification. In the model function of Eq. (8), the mode's feature is parameterized as c. Although we take the mode's feature as parameter irrelevant to the TOA, the basic relation of c and Taylor series coefficients k_1 and k_2 cannot be ignored. k_1 relates to the group velocity v_g, and can be expressed as $k_1 = 1/v_g$. The k_2 is a function of v_g and can be given by $k_2 = -v_g'/\left(2v_g^2\right)$ where the superscript "′" indicates differentiation with respect to frequency. Obviously, as expressed in $g_2(\tau)$, the sign of the c is same as the product of $k_1 \cdot k_2$.

By considering the sign of c, A0 and S0 modes in the low frequency-thickness product region generated by the same excitation can be identified. For a visualized illustration, a typical group velocity for A0 and S0 modes versus the frequency-thickness product in an aluminum plate is given in Fig. 1a. The group velocity of the A0 mode increases or almost remains constant with the frequency-thickness product (under 2000 KHz · mm), but the one of S0 mode consistently decreases. That is, k_2 of A0 mode is non-positive, and the one of S0 mode is positive. Therefore, the mode can be identified by the sign of parameter c.

For better explaining the role of c in featuring the dispersive wave packet, Fig. 1b shows a synthetic signal containing a S0 and an A0 wave packet. While Fig. 1c shows the corresponding time–frequency result obtained by WVD. It can be found, higher-frequency propagates faster than the lower-frequency in the A0-mode while in the S0-mode the higher-frequency propagates slower than the lower-frequency. This is the feature that parameterized by the parameter c.

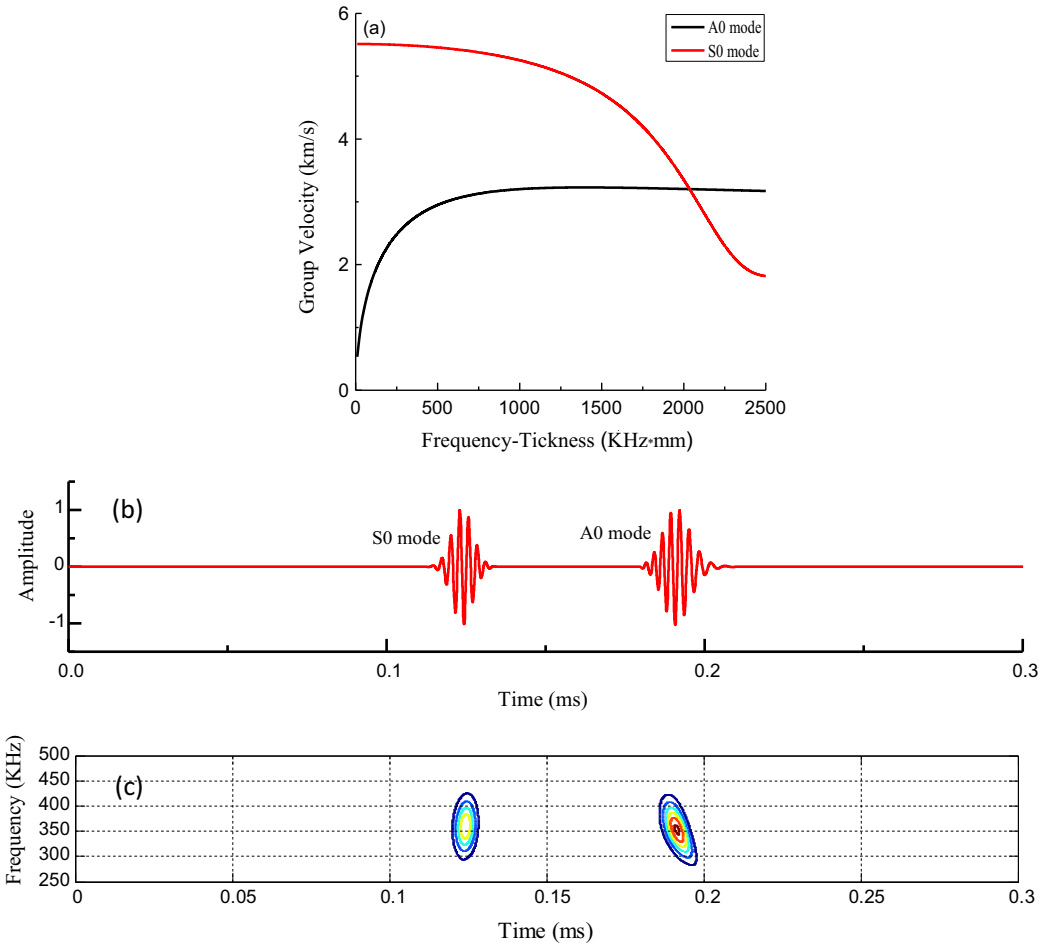

Fig. 1. (a) Group velocity dispersion curve for aluminum. (b) Synthetic signal contains S0 and A0 packets. (c) Time-frequency result obtained by WVD of the synthetic signal in figure (b).

In addition, once the k_1 and k_2 are given, the waveform with the ToA τ in time-domain can be predicted. However, the inverse problem is how to determine the k_1, k_2 from the parameters. Actually, the values of k_1, k_2 cannot be directly obtained from the quantitative parameters, *i.e.* δ, τ and c. As mentioned above, δ equals to $g_1(\tau)$, and $c = g_2(\tau)/2\pi f_c$, thus the Eq. (6) can be written as,

$$\delta = \frac{k_1^2}{k_1^2 + (4\beta\tau k_2)^2}; \quad 2c\pi f_c = \frac{4\beta^2\tau k_2 k_1}{k_1^2 + (4\beta\tau k_2)^2}, \tag{10}$$

then the relation between k_1 and k_2 can be given as

$$\frac{k_2}{k_1} = \frac{2\pi f_c c}{4\beta^2\tau\delta}, \tag{11}$$

For the wave packets with the identical mode, the calculated quotient of k_1, k_2 should be same. Here, we define k_2/k_1 as the *mode identification constant* (*MIC*) to classify wave packets.

2.3. Parameter estimation by the EM algorithm

The observed noisy signal with a number of M superimposed dispersive wave packets can be represented by using Eq. (9),

$$x(t) = y(t) + n(t) = \sum_{m=1}^{M} v(\Theta_m; t) + n(t), \tag{12}$$

where $x(t)$ is the noisy signal (or observed data), $y(t)$ is the noiseless signal, and $n(t)$ represents the noise (White Gaussian noise, WGN). The expansion form of $x(t)$ is,

$$x(t) = \sum_{m=1}^{M} \xi_m \exp\left[-\beta\delta_m \cdot (t-\tau_m)^2\right] \cos\left[2\pi f_c \cdot \left(c_m \cdot (t-\tau_m)^2 + (t-\tau_m)\right) + \varphi_m\right] + n(t). \tag{13}$$

Based on the model, the EM algorithms translate M-superimposed packets estimation into M-separated packets estimations by using unobserved data sets. Consider the added WGN, we define the x_m as the "unobserved data" set of the mth wave packet, and the x_m is

$$x_m = v(\theta_m; t) + n(t), \tag{14}$$

The relation of linear transformation to the observed data is

$$x(t) = \sum_{m=1}^{M} x_m(t), \tag{15}$$

It has been proved that the maximum likelihood estimation (MLE) subjected to the data sets x_m of the parameter vectors Θ_m can be computed, and the MLE of Θ_m maximizes the probability density function (PDF) associated with the data sets x_m. The parameter vectors Θ_m can be estimated by EM algorithm [26,28].

By the Eq. (15), the expectation of current date set x_m associated with Θ_m and observed data can be processed by,

$$\hat{x}_m^{(k)} = v\left(\theta_m^{(k)}\right) + \gamma_m \cdot \left[x - \sum_{l=1}^{M} v\left(\theta_l^{(k)}\right)\right], \tag{16}$$

where $\sum_{m=1}^{M} \gamma_m = 1$, and (k) referred to the number of iteration in the EM algorithm. This is the E-step in EM algorithm, and the maximization step (M-step) utilizes the expectation from E-step to maximize the PDF. In the M-step, the parameter vectors are iterated by minimizing [23]

$$\theta_m^{(k+1)} = \arg_{\theta m}\min \| \hat{x}_m^{(k)} - v(\theta_m) \|^2. \tag{17}$$

This approach based on EM algorithm for parameter estimation for the signal with M-superimposed dispersive packets in WGN can be implemented as following steps:

Step 1. Based on the observed signal, guess the initial parameter vectors and form matrix as $\Theta^{(0)} = \left[\theta_1^{(0)}, \theta_2^{(0)}, \ldots, \theta_M^{(0)}\right]$, then set $k = 0$(iteration number) and $k_{\max} = C$ where C is a nature number stands for the maximum iterations.

Step 2. (E-step) For m = 1,2,. . .,M, compute the expected packets

$$\hat{x}_m^{(k)} = v\left(\theta_m^{(k)}\right) + \gamma_m \cdot \left(x - \sum_{l=1}^{M} v\left(\theta_l^{(k)}\right)\right)$$

in the expression, $\gamma_m = 1/M$, and $v(\theta_l) = \xi_l e^{-\delta_l * (t-\tau_l)^2} \cos\left[2\pi f_c \cdot \left(c_l \cdot (t-\tau_l)^2 + (t-\tau_l)\right) + \varphi_l\right]$ where f_c is the center frequency of the incident pulse.

Step 3. (M-step) For m = 1,2,. . .. M. Iterate the corresponding parameter vector

$\theta_m^{(k+1)} = \arg_{\theta_m}\min \| \hat{x}_m^{(k)} - v(\theta_m) \|^2$ and set $\theta_m^{(k)} = \theta_m^{(k+1)}$. (In this step of our program, a MATLAB function, *nlinfit.m* is used.)

Step 4. Check convergence criteria and iterations: if $\| \Theta_m^{(k+1)} - \Theta_m^{(k)} \| \leqslant$ tolerance or $k \geqslant C$, then stop.

Step 5. Set $k = k + 1$ and go to Step 2.

The above implementation introduces unnecessary calculation, because all parameters are invoked in every iteration calculation. The convergence speed of each wave packet parameter vector is different, and the parameter vector which satisfies the accuracy still needs to be calculated. To improve the computational efficiency, the space alternating generalized EM (SAGE) algorithm can be employed, which convert the M-spike estimation problem into a "one spike at one time" estimation problem [24,25]. It should be note that, for the same initial parameter vectors and observed date, the results obtained by the algorithms are the same. In order to present the results more intuitively, in the following parts, we use the general EM algorithm to process the data.

3. Verifications from synthetic and experimental data

In this section, the studies of synthetic and experimental data are performed. Firstly, for analyzing the convergence and the ability when dealing with dispersive signals, we considered different SR and noise intensities. The experiment contains two parts, the first is to study the impact of excitation pulse bandwidth on the accuracy of the reconstructed signals. The second, the ability of mode identification and time locating are verified. Additionally, the group velocity curves are also estimated with the parameters.

3.1. Study of synthetic signals

Generally, the convergence and speed of EM algorithm are related to the SR and the sampling length of the signal. Here, we used an excitation of Gabor pulse with the bandwidth factor of 3.25E−6 and center frequency of 360 KHz. For studying the accuracy of results, we associated the dispersion relation as shown in Fig. 1a (the k_1 for A0 and S0 are 3.21E−4 and 1.855E−4; the k_2 are −2.55E−11 and 6.429E−12, respectively.) with the model function Eq. (8), and synthesized dispersive signals of a 2 mm thick aluminum plate as shown in Fig. 2a. These signals synthesized with the same parameter vectors and different SRs. In the study, the cases of single A0, S0 packet and A0-S0 overlapping packet were considered. Where, the S01/A01 is the direct arrival of S0/A0 mode, and the S02/A02 is the wave packet reflected by the left boundary. In addition, WGN with −30 dBW (using a MATLAB function *wgn*) is added to all signals. Fig. 2b and 2c shows the synthetic noiseless signal and noisy signal, and the corresponding parameter vectors were listed in the Table 1 which be used for evaluating the accuracy of results. By observing the signal, we guessed the initial parameter vectors listed in the Table 2. Fig. 3 plotted the convergence history of the parameter c of S01 and the $\| \Theta_m^{(k+1)} - \Theta_m^{(k)} \|$, respectively. And all the parameter results were listed in the Table 3.

By comparing the predefined parameters and the convergence results in Fig. 3b, we can find that, except the case of SR = 1E6 Hz, all the results are desirable. The confusing results of the case SR = 1E6 Hz can be attributed to the effect of over-fitting. That is, too small sampling length to represent the predefined model accurately. The tolerance results in Fig. 3b indicate that the larger sampling length may lead to fewer iterations. However, the larger sampling length, the more computation. To examine the relationship between them, we evaluated the tolerance threshold as 1E−8, the number of iterations and the operation time were listed in Table 4 (the hardware information: CPU, Intel Core i7–5600U and RAM, 8 GB).

As an extended application in the modal conversion cases, we need to classify the wave packets base on the dispersion relation characteristic, *i.e.* obtaining the *MIC*. The calculated results of the *MIC* in the case of SR = 10E6 Hz were shown in Fig. 4. It should be noted that, the *MIC* of the wave packets with the identical mode approximate to the same value.

To further investigate the noise resistance performance, as shown in Fig. 5, we synthetized signals (SR = 10E6 Hz) which added with WGN of different intensities (−25 dBW, −20 dBW, −15 dBW and −10 dBW). With the same procedures, parameter results of the overlapping packets, *i.e.* A01 and S02, were given in the Table 5. Except the case of −10 dBW, the other values are well; and the results of the case of −10 dBW are acceptable. However, the acceptable results were carried out by taking the values in the Table 2 as the initial parameter vectors, and it is almost impossible to guess appropriate initial parameter vectors from the signal in the Fig. 5. In the case of −15 dBW (the area of 60–90 μs), the overlapping wave packets are immersed in severe noise, but can be observed. Therefore, the appropriate initial parameter vectors can be guessed. Overall, the results reveal the good anti-noise capability of the method, but the signal noise should be limited to guess the appropriate initial parameters.

3.2. Study on the impact of excitation bandwidth on the signal reconstruction

The essence of the general non-linear frequency dispersion theory is to use a two order polynomial to express the dispersion relation of a narrowband signal. The accuracy mainly depends on the bandwidth and the central frequency of excitation pulse. The relation between the group velocity and frequency is $v_g = 1/k_1 = \partial\omega/\partial k$, where the ω is angular frequency and k is the wave number, and $v_g' = -2v_g^2 k_2$ [16]. Thus, with the conception of general non-linear frequency dispersion theory, the group velocity curve near the center frequency can be approximately presented by a linear equation.

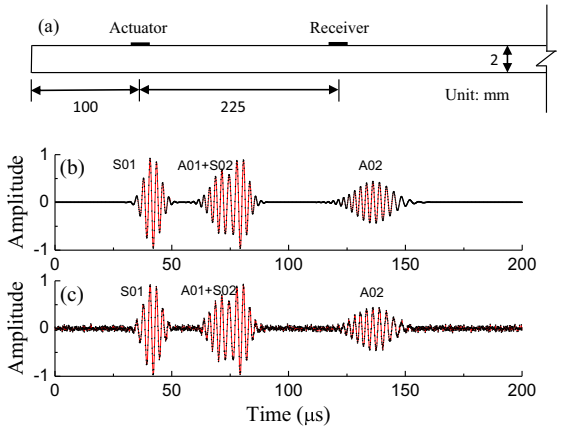

Fig. 2. (a) Plate model used for synthetizing signals. (b) Synthetic noiseless signal. (c) Synthetic signal added with WGN.

Table 1
Parameter vectors used for synthesizing the signal.

	S01	A01	S02	A02
ξ	0.964	0.677	0.888	0.438
δ	0.930	0.459	0.79	0.192
$\tau(\mu s)$	41.74	72.23	78.84	136.43
$c(10^4)$	0.533	−1.043	0.854	−0.824
0.459φ	2.3	1.9	1.8	0.7

Table 2
The guessed initial parameter vectors.

	Wave packet 1	Wave packet 2	Wave packet 3	Wave packet 4
ξ	1	0.8	0.8	0.5
δ	0.6	0.6	0.6	0.4
$\tau(\mu s)$	40	70	80	135
$c(10^4)$	1	1	0.8	0.8
φ	1	1	1	1

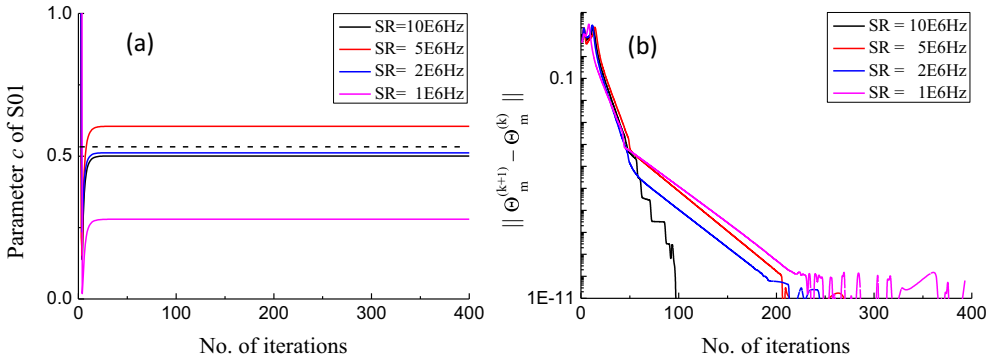

Fig. 3. Each iteration results of the signal with different sampling rate. (a) Results of parameter c of S01. Where, the dash lines in the figures stand for the defined values. (b) Results of $\| \Theta_m^{(k+1)} - \Theta_m^{(k)} \|$.

Table 3
Parameters of each packet after 400 iterations.

	S01					A01				
	ξ	δ	τ	c	φ	ξ	δ	τ	c	φ
SR = 10E6	0.961	0.904	41.71	0.507	2.25	0.674	0.452	72.30	−0.988	1.95
SR = 5E6	0.954	0.898	41.72	0.605	2.25	0.689	0.481	72.26	−1.072	1.98
SR = 2E6	0.970	0.909	41.78	0.511	2.41	0.699	0.449	72.38	−1.064	2.27
SR = 1E6	0.965	0.940	41.67	0.279	2.14	0.733	0.410	72.72	−1.015	3.06
	S02					A02				
	ξ	δ	τ	c	φ	ξ	δ	τ	c	φ
SR = 10E6	0.889	0.807	78.85	0.824	1.82	0.442	0.204	136.43	−0.821	0.71
SR = 5E6	0.899	0.810	78.85	0.793	1.84	0.451	0.194	136.47	−0.846	0.82
SR = 2E6	0.902	0.777	78.63	0.824	1.32	0.445	0.200	136.43	−0.814	0.72
SR = 1E6	0.940	0.936	78.35	0.645	0.61	0.400	0.176	136.41	−0.773	0.61

Table 4
Number of iterations and operation time.

	SR = 10E6 Hz	SR = 5E6 Hz	SR = 2E6 Hz
Number of iterations	148	152	131
Operation time (s)	12.94	9.69	6.48

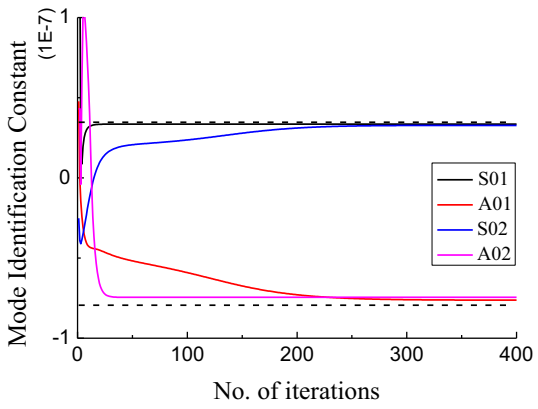

Fig. 4. Mode identification constant (*MIC*) results.

As shown in Fig. 6a, the black line is the group velocity curve of S0 mode, and the color lines are the fitting results (least square fitting) under different bandwidth conditions, and the center frequencies all are 300 KHz (a point near the $v_g'' = 0$). Here, we define the error ($E_{\text{A-F}}$) to evaluate the difference between the actual value and the fitted value, and the $E_{\text{A-F}}$ is

$$E_{\text{A-F}} = 1 - \frac{\int_{f_0}^{f_1} D_T(f) D_P(f) \mathrm{d}f}{\sqrt{\int_{f_0}^{f_1} D_T(f)^2 \mathrm{d}f \int_{f_0}^{f_1} D_P(f)^2 \mathrm{d}f}}, \tag{18}$$

where the f is the frequency. Fig. 6b plots the $E_{\text{A-F}}$ vary with bandwidth. It can be found that, with the decrease of bandwidth, the $E_{\text{A-F}}$ decreases. It is mainly due to the effect of higher-order terms, which decreases with the bandwidth's decrease.

In order to verify the trend of the actual cases, we adopted excitation pulses with different bandwidth and compared the first arrival wave packet in the measured signals and the reconstructed signals. As shown in Fig. 7a, a pair of piezoelectric wafer (PZT) with thickness of 0.5 mm and diameter of 8 mm were bonded on the top surface of a 2 mm thick aluminum plate. The distance between the wafers is 450 mm. As shown in Fig. 7b, an analog output card (PCI-1721) and a data acquisition card (PCI-1714U) were used for signal output and input. The analog output card is connected to a power amplifier (ATA-2022), and the amplified excitation signal powers the actuator. The control system and the digital band-pass filtering (100 KHz–720 KHz) are implemented by a program of National Instrument LabVIEW. In the experimental system, the analog output and data acquisition cards were synchronized to make sure that the excitation and the data acquisition started at the same time.

The central frequency of all the excitation signals is 300 KHz, and the bandwidths were controlled by the σ. The Fig. 8a plots the waveforms of the excitation signals, and the Fig. 8b gives the corresponding results of Fourier transform (FT). With the increase of σ, the bandwidth decreases. The Fig. 8c plots the waveforms of first arrival (S0 mode) in the measured and reconstructed signals. Similar as the definition of $E_{\text{A-F}}$ introduced above, the deviation $D_{\text{O-R}}$ between original signal and reconstructed signal can be calculated as

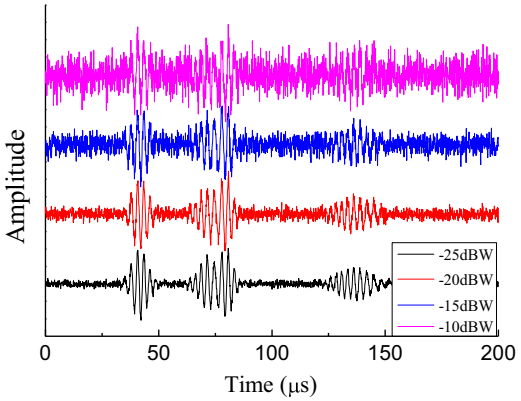

Fig. 5. Synthetic signals added with WGN of different intensities.

Table 5
Iteration results of synthetic signals with different intensities of noise.

	A01					S02				
	ξ	δ	τ	c	φ	ξ	δ	τ	c	φ
−25 dBW	0.718	0.465	72.51	−1.031	2.00	0.917	0.776	78.50	0.877	1.82
−20 dBW	0.635	0.417	72.12	−1.089	2.16	0.897	0.850	78.99	0.894	1.63
−15 dBW	0.630	0.537	72.24	−1.119	2.40	0.930	0.857	79.07	0.814	1.94
−10 dBW	0.587	0.348	72.44	−1.003	2.42	0.872	0.650	78.85	1.013	1.69

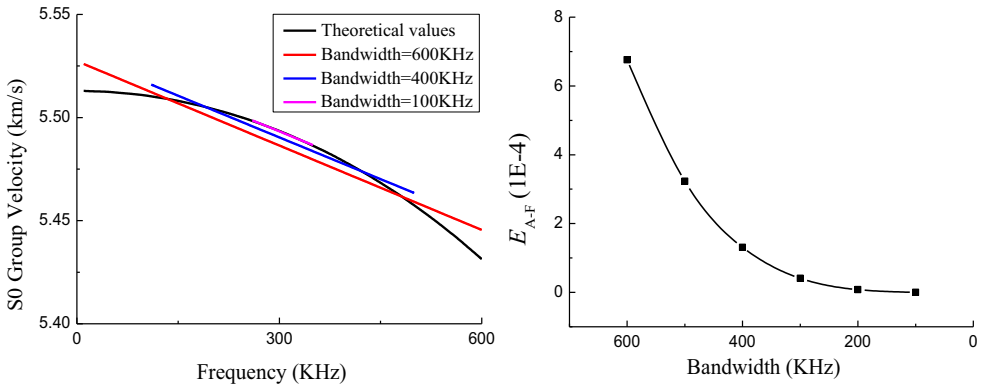

Fig. 6. (a) Comparison between the theoretical and fitted group velocity curves of S0 mode in a 1 mm aluminum plate. (b) $E_{A\text{-}F}$ decrease with the decrease of the excitation pulse bandwidth.

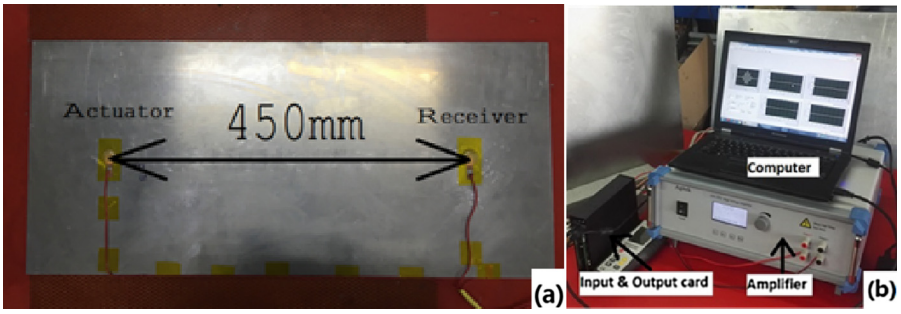

Fig. 7. (a) Aluminum plate used for sampling Lamb wave signals. (b) Experimental setups.

$$D_{\text{O-R}} = 1 - \frac{\int_{t_0}^{t_1} M_O(t) M_P(t) \mathrm{d}t}{\sqrt{\int_{t_0}^{t_1} M_0(t)^2 \mathrm{d}t \int_{t_0}^{t_1} M_P(t)^2 \mathrm{d}t}}, \tag{19}$$

The $D_{\text{O-R}}$ result of each experimental case is drawn in the Fig. 8d, which indicates that the narrower bandwidth means the smaller deviation. This trend is similar to the analysis of the group velocity (as shown in the Fig. 6b), which means the narrowband excitation pulse is necessary for the application of the general non-linear frequency dispersion theory.

3.3. Analysis of experimental data

As shown in Fig. 9, a 1.82 mm thick aluminum plate (type-2024 with material parameters, density: $\rho = 2700\ \text{kg/m}^3$, Young's modulus: E = 73.1GPa, and the Poisson ratio is 0.33) with the in-plane dimension of $650 \times 600\ \text{mm}^2$ is used in our experimental verification. Two identical piezoelectric wafers (PZT) used as actuator and receiver, were bonded to the top surface of the sample. The thickness across the wafer is 0.5 mm, and the diameter is 10 mm. The excitation signal is the same as which in the study of synthetic signals, *i.e.*, a Gabor pulse with the bandwidth factor of 3.25e−6 and the center frequency of 360 KHz.

The detected signal with the sampling rate of 10 MHz, containing wave packets with different amplitude, was shown in Fig. 10. In the region of 0–120 μs, there are four obvious individual packets. In the region of 120–150 μs, a possible single

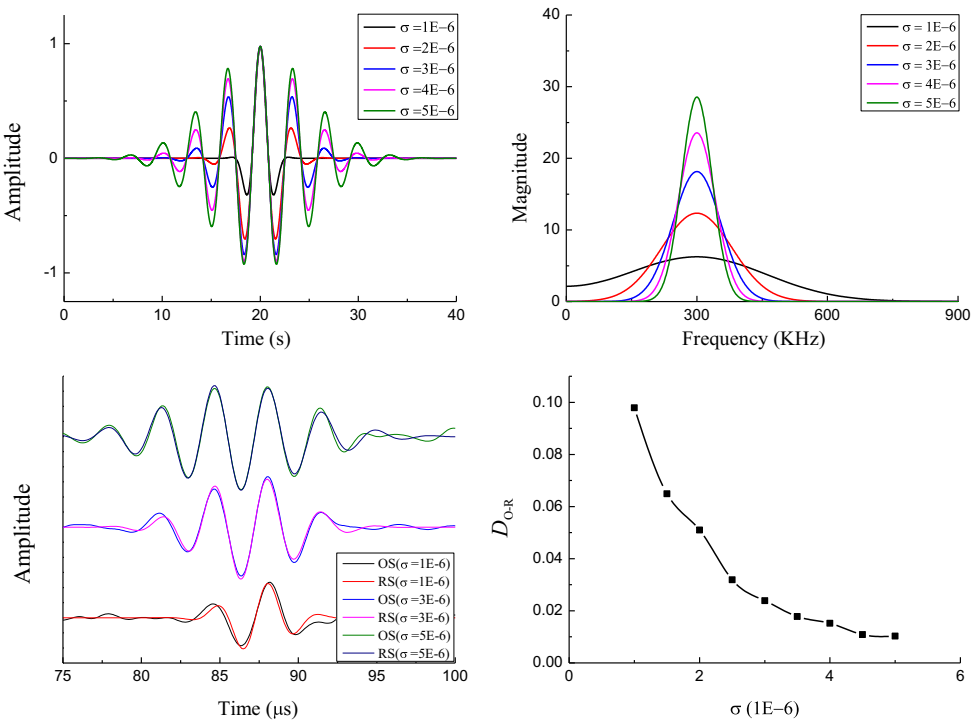

Fig. 8. (a) Waveforms of Gabor pulse with variation bandwidth factor σ. (b) Corresponding FT results of excitation pulse. (c) The first arrival wave packet of reconstructed signals (RS) and original signals (OS) under excitation pulse with different σ. (d) $D_{O\text{-}R}$ between the original signals and the reconstructed signals.

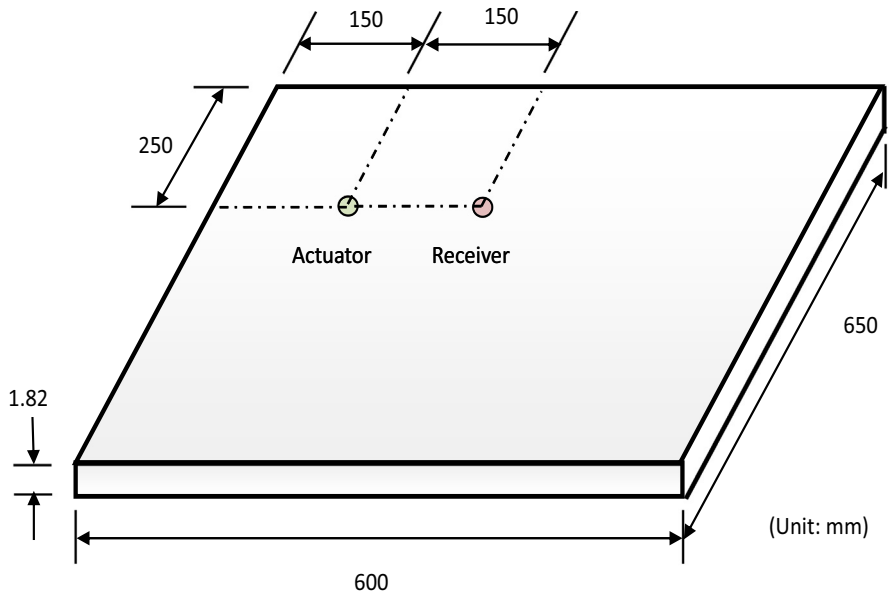

Fig. 9. Experimental setup for detecting Lamb wave signal in an aluminum plate.

packet appears, but the boundaries and the amplitude indicate that it may be an overlapping packet that consists of an S0 and an A0 packet. The region of 150–210 μs apparently contains three packets, and at least four packets should be in the region of 210–300 μs. Based on the observed data, the guessed initial parameter vectors were obtained and be listed in the Table 6.

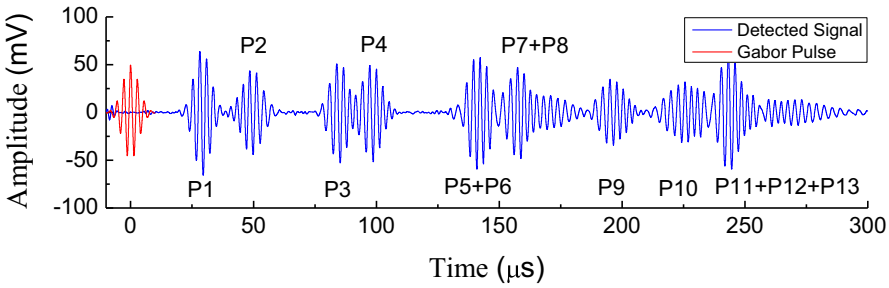

Fig. 10. Detected signal contains wave packets with different amplitude in blue line and Gabor pulse with peak-to-peak amplitude of 36 V in red line. (For interpretation of the references to color in this figure legend, the reader is referred to the web version of this article.)

Table 6
The guessed initial parameter vectors to the detected signal.

	P.1	P2	P3	P4	P5	P6	P7	P8	P9	P10	P11	P12	P13
ξ	65	45	52	50	30	30	50	30	35	50	25	20	20
δ	0.9	0.6	0.8	0.75	0.65	0.3	0.5	0.3	0.5	0.4	0.2	0.3	0.2
$\tau(\mu s)$	28	50	80	95	140	145	155	170	195	225	240	245	265
$c(10^4)$	0.5	−0.9	0.9	0.9	1	−0.8	1.0	−0.7	1	1	−0.8	1	−0.5
φ	0	0	0	0	0	0	0	0	0	0	0	0	0

Table 7
Iteration result of the parameter vectors in the detected signal.

	P.1	P2	P3	P4	P5	P6	P7	P8	P9	P10	P11	P12	P13
ξ	66.2	44.6	53.3	51.3	44.5	22.6	45.7	17.2	35.1	31.9	42.3	39.5	13.1
δ	0.96	0.60	0.77	0.71	0.63	0.50	0.73	0.13	0.39	0.27	0.84	0.18	0.07
$\tau(\mu s)$	29.3	49.5	85.0	98.4	141.2	143.2	156.9	169.3	196.2	224.5	243.6	244.3	268.0
$c(10^4)$	0.28	−1.02	0.86	0.97	1.17	−1.58	1.19	−0.70	1.01	0.93	−0.08	0.83	−0.45
φ	2.26	−4.04	8.61	8.63	3.28	−3.61	4.93	−3.79	2.30	−2.83	6.17	−3.37	7.27

We obtained the parameter vectors listed in Table 7 after 1000 times of iteration. Fig. 11a shows the convergence history of $\| \Theta_m^{(k+1)} - \Theta_m^{(k)} \|$. The reconstructed signal that utilizing the parameters in Table 7 is given in Fig. 11b, and we can note that the calculated signal can represent the detected signal well. The *MIC* results, *i.e.* shown in Fig. 11c, indicate the packets of 1, 3, 4, 5, 7, 9, 10 and 12 can be classified into the same mode, *i.e.* S0 mode; and the packets of 2, 6, 8 and 13 can be classified into another mode, *i.e.* A0 mode. By evaluating the value of *MIC*, the mode type of packet 11 is uncertain; with the sign of $k_1 \cdot k_2$, packet 11 can be classified into A0 mode. Additionally, the *MIC* results of S0 mode concentrate better than the A0 mode. That mainly because that under the same bandwidth, the higher order terms impact more obviously on the A0-mode than the S0-mode.

To qualitatively analyze the results, we estimated the propagation path of each wave packet in the signal. As shown in Fig. 12, taking the locations of actuator and receiver as point 0 and 1, the propagation paths and distances can be estimated as follows, No.1 (0-1, 150 mm), No.2 (0-2-1, 450 mm), No.3 (0-3-1, 522.02 mm), No.4 (0-4-1, 750 mm), No.5 (0-5-1, 831.94 mm), No.6 (0-2-4-1, 1050 mm), No.7 (0-4-2-1, 1200 mm), No.8 (0-6-9-1, 1308.6 mm) and No.9 (0-7-8-1, 1308.6 mm). Due to the same distances along the path of No.8 and No.9, the actual number of paths is eight. With the distance from the path of No.1 and the ToA of first two packets (*i.e.* the direct arrival of S0 and A0), the group velocity can be calculated as 5119.5 m/s and 3030.3 m/s. With the above information, we compared the estimation and calculation ToA results as shown in Fig. 13a (where the sign(c) > 0 stands for the S0 mode and sign(c) < 0 stands for the A0 mode). However, the error increases with time, and may be induced by the inaccurate group velocity caused by the system delay. The system delay might be caused by two possible reasons. One is the delay between the analog output card and the data acquisition card; the other is the delay between the analog output card and the power amplifier. Therefore, basing on the time difference between the two wave packets (P1 and P3, P2 and P8) and their distance difference, we re-calculate the group velocity. The group velocity for S0 is 5386.0 m/s and for A0 is 3105.3 m/s, respectively, and the comparison is shown in Fig. 13b where the error between estimation and calculation mainly caused by the system delay, so we took the ToA of P1 in both estimation

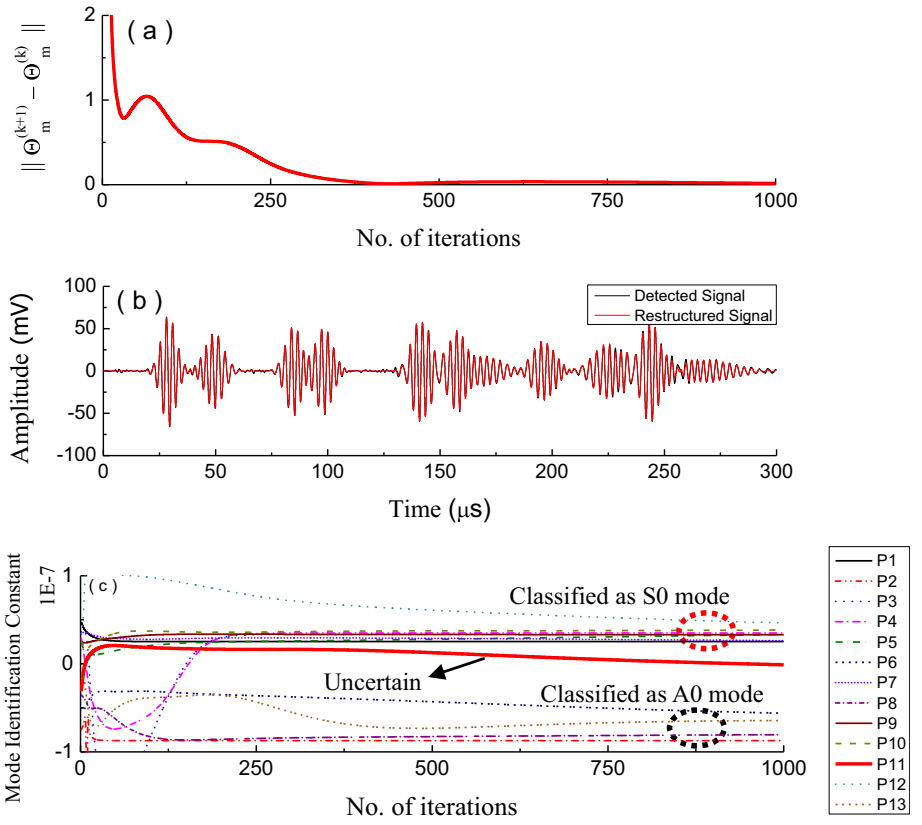

Fig. 11. Iteration results. (a) $\| \Theta_m^{(k+1)} - \Theta_m^{(k)} \|$ against the number of iterations. (b) The comparison between the detected signal and the restructured signal. (c) Mode identification constant versus the number of iterations.

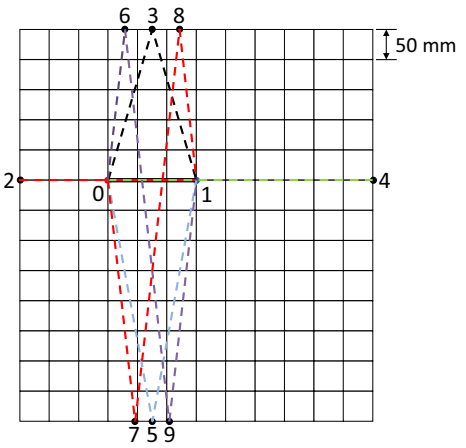

Fig. 12. Estimated propagation path in the aluminum plate.

and calculation as the zero point. The comparison can be performed as Fig. 13c. All the results match well, except the ToA of P6 and P13.

With the estimated group velocities (v_g) of S0 and A0, the corrected ToA, and the relation between the v_g' and k_1, k_2, the corresponding group velocity curves around the center frequency can be estimated. From the *MIC*, *i.e.* Eq. (11), the k_2 can be expressed by

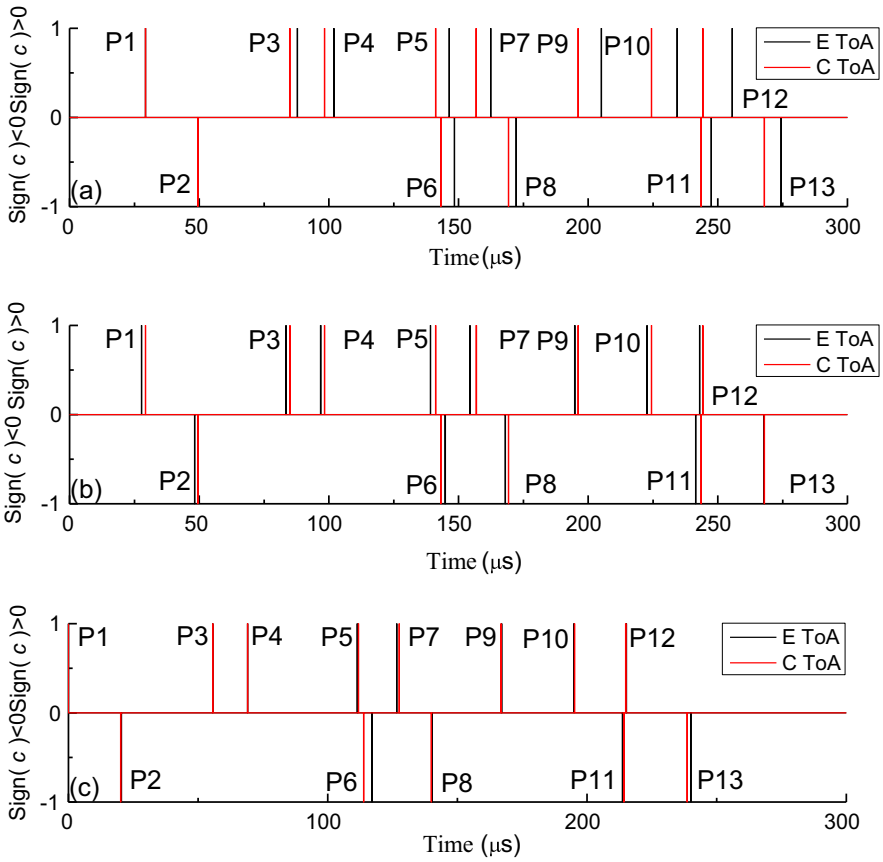

Fig. 13. Comparison between estimated ToA and calculation ToA. (a) Group velocity calculated according to the ToA of P1, P2 and propagation path No.1. (b) Group velocity of S0 mode calculated according to the ToA of P1, P3 and distance difference between path No.1 and No.2; Group velocity of A0 mode calculated according to the ToA of P2, P8 and distance difference between path No.1 and No.3. (c) System delay eliminated.

$$k_2 = \frac{2\pi f_c c}{4\beta^2 \tau \delta} k_1, \tag{20}$$

And combine the relation of $k_2 = -v_g'/\left(2v_g^2\right)$ and $k_1 = 1/v_g$, we can get

$$v_g' = -\frac{\pi f_c c}{\beta^2 \tau \delta} v_g, \tag{21}$$

Then the v_g' of P1 and P2 can be obtained as −2.822E−4 and 5.516E−4 (unite: m/(Hz·mm·s)), respectively. Fig. 14a plots the estimated and theoretical curves. In the available Frequency-thickness area (estimated by the half-peak of power spectral density (PSD) of the excitation signal), the two curves are well coincident, and the $E_{A\text{-}F}$ of S0 and A0 are 0.17E−4 and 9.3E−4, respectively. The Fig. 14b and c plot the details of the curves. Additionally, the fitted straight lines which are based on the data of the theoretical curves are also given, and the v_g' of the lines are −3.061E−4 (S0) and 5.517E−4 (A0), respectively. For the A0 mode, the difference mainly is the velocity; and the estimation of v_g' performs much better than the S0.

By analyzing the data above, the conclusions can be derived as follows. (1) For the single packet (*i.e.* P1, P2, P3, P4, P9 and P10 in the signal), both the results of ToA and *MIC* are desirable. (2) For the case that two wave packets almost completely overlapped (*i.e.* the case of P5 + P6), the *MIC* and the sign of *c* can be available, but the ToA may be disturbed. (3) For the overlapping packets with the bigger time difference (*i.e.* the case of P7 + P8), both credible ToA and *MIC* can be obtained. (4) With the increase of overlapping wave packets (*i.e.* the case of P11 + P12 + P13), the *MIC* of some/all packets are unreliable. (5) The estimated group velocity curves can present the dispersion relation in a finite area which near the center frequency.

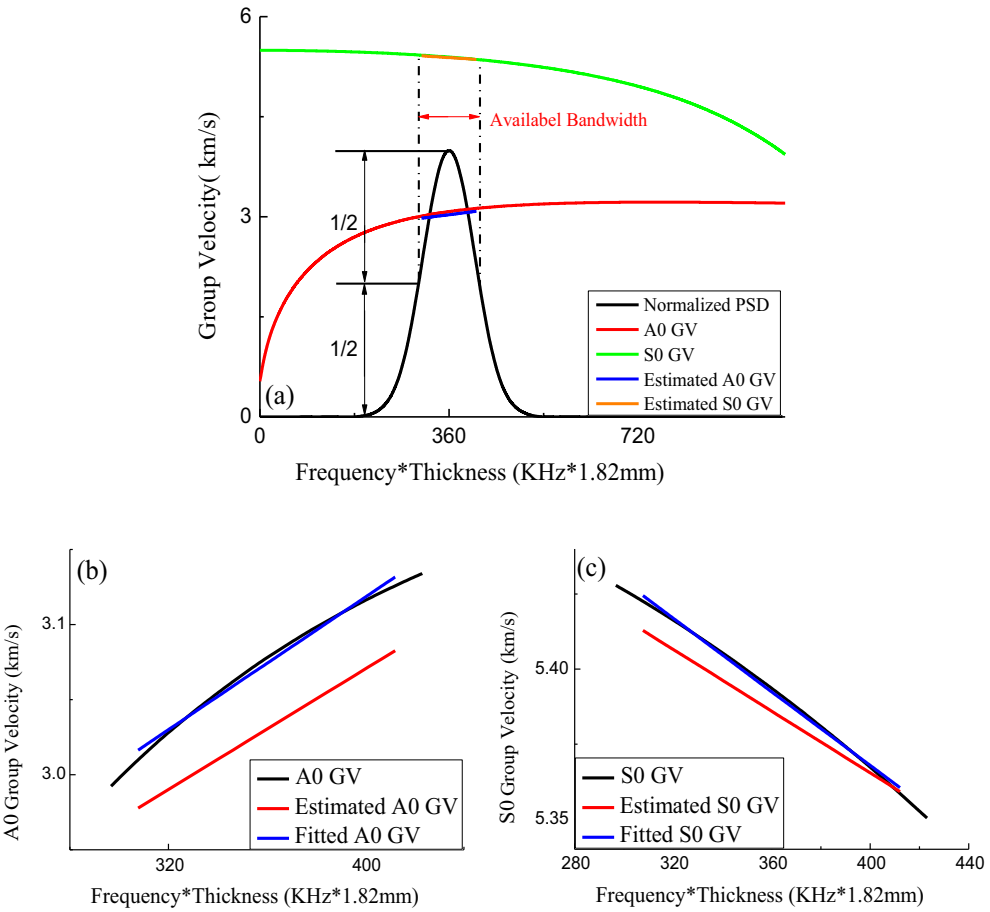

Fig. 14. The comparisons of group velocities of A0 and S0 mode in an aluminum plate with thickness of 1.82 mm. (a) Comparisons between the estimated group velocity curves and theoretical values in the available area. (b), (c) Details of theoretical GV, estimated GV and fitted GV in the available area for A0, S0 mode, respectively.

4. Conclusion

In this study, we developed an approach based on EM algorithm for Lamb wave signal processing. By using the narrowband Gabor pulse as the excitation signal, the model function of the dispersive waveform was derived. With the obtained parameters, the *MIC* for the wave packet classification can be further calculated. In the study of synthetic signals, the convergence and speed were examined. The accuracy and feasibility of the parameters were further discussed by the experiments.

This technique can be used to extract ToA and mode information from the wave packets with unknown dispersion relation. The extracting of ToA in wave packets is the fundamental step for Lamb wave inspection; the classification of wave packets can make it convenient for Lamb wave signals analyzing. It should be noted that, in the cases of anisotropic materials the dispersive time–frequency trends vary constantly, and using a specific *MIC* to classify the wave packets is inaccurate. Using the approach proposed several merits in SHM/NDE for damage locating and identification can be summarized as: (1) The ToA is an approximated constant which can provide a high resolution to locate damage. (2) The adoption of the excitation frequency region is relaxed, *i.e.* the excitation frequency in a non-dispersive region is not essential. (3) Wave packet modes can be classified by *MIC*, which can avoid the uncertainty caused by multimode in the process of signal analysis. Additionally, the current approach may need much calculation, and the risk of over-fitting may produce a confused the results.

Acknowledgement

This work is supported by the Foundation for Innovative Research Groups of the National Nature Science Foundation of China (Grant No. 11421091) and Special Funds for Scientific and Technological Innovation Talents of Harbin (Grant No. JJ20170379).

References

[1] J.L. Rose, P.B. Nagy, Ultrasonic waves in solid media, J. Acoust. Soc. Am. 107 (2000) 1807–1808.
[2] P. Cawley, D. Alleyne, The use of Lamb waves for the long range inspection of large structures, Ultrasonics 34 (1996) 287–290.
[3] T. Ghosh, T. Kundu, P. Karpur, Efficient use of Lamb modes for detecting defects in large plates, Ultrasonics 36 (1998) 791–801.
[4] P. Wilcox, M. Lowe, P. Cawley, The effect of dispersion on long-range inspection using ultrasonic guided waves, NDT& E Int. 34 (2001) 1–9.
[5] J. Moll, R.T. Schulte, B. Hartmann, et al, Multi-site damage localization in anisotropic plate-like structures using an active guided wave structural health monitoring system, Smart Mater. Struct. 19 (2010) 126–134.
[6] Z. Su, X. Wang, Z. Chen, et al, A hierarchical data fusion scheme for identifying multi-damage in composite structures with a built-in sensor network, Smart Mater. Struct. 16 (2007) 2067–2079.
[7] N. Hu, T. Shimomukai, C. Yan, et al, Identification of delamination position in cross-ply laminated composite beams using S0 Lamb mode, Compos. Sci. Technol. 68 (2008) 1548–1554.
[8] B. Wu, Y. Huang, X. Chen, et al, Guided-wave signal processing by the sparse Bayesian learning approach employing Gabor pulse model, Struct. Health Monit. 16 (2017) 347–362.
[9] J. Hong, K.H. Sun, Y.Y. Kim, Dispersion-based short-time Fourier transform applied to dispersive wave analysis, J. Acoust. Soc. Am. 117 (2005) 2949–2960.
[10] M. Niethammer, L.J. Jacobs, J. Qu, et al, Time-frequency representations of Lamb waves, J. Acoust. Soc. Am. 109 (2001) 1841–1847.
[11] Y.Y. Kim, E. Kim, Effectiveness of the continuous wavelet transform in the analysis of some dispersive elastic waves, J. Acoust. Soc. Am. 110 (2001) 86–94.
[12] H. Jeong, Y. Jang, Fracture source location in thin plates using the wavelet transform of dispersive waves, IEEE Trans. Ultrason. Ferroelectr. Freq. Control 47 (2000) 612–619.
[13] S.T. Quek, P.S. Tua, Q. Wang, Detecting anomalies in beams and plate based on the Hilbert-Huang transform of real signals, Smart Mater. Struct. 12 (2003) 447–460.
[14] P.D. Wilcox, A rapid signal processing technique to remove the effect of dispersion from guided wave signals, IEEE Trans. Ultrason. Ferroelectr. Freq. Control 50 (2003) 419–427.
[15] Z. Luo, L. Zeng, J. Lin, et al, A reshaped excitation regenerating and mapping method for waveform correction in Lamb waves dispersion compensation, Smart Mater. Struct. 26 (2017) 025016.
[16] L. Liu, F.G. Yuan, A Linear mapping technique for dispersion removal of Lamb waves, Struct. Health Monit. 9 (2010) 75–86.
[17] J. Cai, S. Yuan, X.P. Qing, et al, Linearly dispersive signal construction of Lamb waves with measured relative wave number curves, Sens. Actuators, A 221 (2015) 41–52.
[18] C. Xu, Z. Yang, X. Chen, et al, A guided wave dispersion compensation method based on compressed sensing, Mech. Syst. Signal Procss. 103 (2018) 89–104.
[19] J. Hong, K.H. Sun, Y.Y. Kim, The matching pursuit approach based on the modulated Gaussian pulse for efficient guided-wave damage inspection, Smart Mater. Struct. 14 (2005) 548.
[20] J. Hong, K.H. Sun, Y.Y. Kim, Waveguide damage detection by the matching pursuit approach employing the dispersion-based chirp functions, IEEE Trans. Ultrason. Ferroelectr. Freq. Control 53 (2006) 592–605.
[21] L.D. Marchi, M. Ruzzene, B. Xu, et al, Warped basis pursuit for damage detection using Lamb waves, EEE Trans. Ultrason. Ferroelectr. Freq. Control 57 (2010) 2734–2741.
[22] S. Agarwal, M. Mitra, Lamb wave based automatic damage detection using matching pursuit and machine learning, Smart Mater. Struct. 23 (2014) 085012.
[23] J. Moll, C. Heftrich, C.P. Fritzen, Time-varying inverse filtering of narrowband ultrasonic signals, Struct. Health Monit. 10 (2011) 403–415.
[24] D. Ramazan, S. Jafar, Model-Based estimation of ultrasonic echoes part I: analysis and algorithms, IEEE Trans. Ultrason. Ferroelectr. Freq. Control 48 (2001) 787–802.
[25] D. Ramazan, S. Jafar, Model-Based estimation of ultrasonic echoes part II: nondestructive evaluation applications, IEEE Trans. Ultrason. Ferroelectr. Freq. Control 48 (2001) 803–811.
[26] B. Abdessalem, D. Redouane, G. Abderrezak, Detection of delamination defects in CFRP materials using ultrasonic signal processing, Ultrasonics 48 (2008) 731–738.
[27] P. Alessandro, D.I. Tommaso, M. Alessandro, et al, Model-based compressive sensing for damage localization in lamb wave inspection, IEEE Trans. Ultrason. Ferroelectr. Freq. Control 60 (2013) 2089–2097.
[28] F. Meir, W. Ehud, Parameter estimation of superimposed signals using the EM algorithm, IEEE Trans. Signal Process. 36 (1988) 477–489.